Numerical study of the tight-binding approach to overdamped Brownian motion on a tilted periodic potential

K. J. Challis
Scion, 49 Sala Street, Private Bag 3020, Rotorua 3046, New Zealand
(Received 1 May 2016; revised manuscript received 29 November 2016; published 19 December 2016)

We present a numerical study of the tight-binding approach to overdamped Brownian motion on a tilted periodic potential. In the tight-binding method the probability density is expanded on a basis of Wannier states to transform the Smoluchowski equation to a discrete master equation that can be interpreted in terms of thermal hopping between potential minima. We calculate the Wannier states and hopping rates for a variety of potentials, including tilted cosine and ratchet potentials. For deep potential minima the Wannier states are well localized and the hopping rates between nearest-neighbor states are qualitatively well described by Kramers' escape rate. The next-nearest-neighbor hopping rates are negative and must be negligible compared to the nearest-neighbor rates for the discrete master equation treatment to be valid. We find that the validity of the master equation extends beyond the quantitative applicability of Kramers' escape rate.

DOI: 10.1103/PhysRevE.94.062123

I. INTRODUCTION

Brownian motion on a tilted periodic potential is a text-book problem for studying nonequilibrium transport in periodic systems dominated by thermal fluctuations [1,2]. The standard theoretical description of Brownian motion on tilted periodic potentials is based on a continuous diffusion equation [1]. That equation can be solved exactly in one dimension for the steady state [1–3] and can be made tractable in certain other limits by analytic methods [1,4]. In particular, for potentials with deep minima, simpler master equation treatments have been used [4,5]. Attempts have been made to connect the continuous diffusion equation with discrete approaches [6–12], but the assumptions inherent in discrete treatments are not always made explicit. Recently, we transformed the continuous diffusion equation to a discrete master equation by implementing the classical analog of the tight-binding model of quantum mechanics [13,14]. The key advantage of this approach is that the master equation is derived systematically, making clear the approximations applied [13,14]. In this paper, we present a detailed numerical study of these approximations to determine the validity of the tight-binding approach to Brownian motion on periodic and tilted periodic potentials.

In the tight-binding method the probability density is expanded on a basis of Wannier states to derive a master equation that can be interpreted in terms of discrete thermal hopping between potential minima [13,14]. Three approximations are made in the derivation. Approximation (A1): The eigenvalues of the evolution operator separate into bands enabling a separation of time scales and a lowest-band description in the long-time limit. Approximation (A2): The Wannier states are localized so hopping between nearest-neighbor states dominates and higher-order transitions between non-nearest-neighbor states are neglected. Approximation (A3): The connection with Kramers' problem of thermal escape over a potential barrier [4,14–16] means that hopping rates between nearest-neighbor Wannier states are given by Kramers' escape rate [14]. In this paper, we consider the validity of these approximations for a variety of potentials including cosine and ratchet potentials and tilted periodic potentials. We calculate the lowest band gap in the eigenvalue spectrum and find the tilt where the gap vanishes. We calculate the Wannier states and determine their localization. We calculate the hopping rates between states and compare the nearest-neighbor hopping rates with Kramers' escape rate. We also determine the importance of higher-order hopping rates in the master equation. To clarify the validity of the discrete master equation description and the applicability of Kramers' escape rate, we focus on one-dimensional systems. However, the tight-binding method is applicable in higher dimensions and we illustrate this by considering a simple two-dimensional case.

This paper is organized as follows. In Sec. II we introduce the one-dimensional continuous diffusion equation for overdamped Brownian motion on a tilted periodic potential. In Sec. III we summarize the tight-binding approach. In Sec. IV we describe our numerical method and detail the one-dimensional periodic potentials considered in this paper. In Secs. V and VI we study the system with untilted and tilted periodic potentials, respectively. In Sec. VII we discuss the validity of the tight-binding approach. In Sec. VIII we calculate the ground state and average drift using the tight-binding approach and make a comparison with the exact steady-state results. In Sec. IX we consider a tilted periodic potential in two dimensions. We conclude in Sec. X.

II. OVERDAMPED BROWNIAN MOTION ON A TILTED PERIODIC POTENTIAL

Overdamped Brownian motion of a particle on a one-dimensional tilted periodic potential can be described by the Smoluchowski equation

$$\frac{\partial P(x,t)}{\partial t} = \mathcal{L}P(x,t), \tag{1}$$

where $P(x,t)$ is the probability density of finding the particle at position x at time t [1]. The evolution operator is

$$\mathcal{L} = \frac{1}{\gamma}\frac{\partial}{\partial x}\left[\Theta\frac{\partial}{\partial x} - F(x)\right], \tag{2}$$

where γ is the friction coefficient, $\Theta = k_B T$, k_B is the Boltzmann constant, and T is the temperature. The force

$F(x)$ is the negative gradient of the tilted periodic potential $V(x)$, i.e.,

$$F(x) = -\frac{\partial V(x)}{\partial x}, \tag{3}$$

$$V(x) = V_0(x) - fx, \tag{4}$$

$$V_0(x) = V_0(x+a), \tag{5}$$

where a is the periodicity of the periodic potential $V_0(x)$ and f is the tilt.

The Smoluchowski equation [Eq. (1)] for a tilted periodic potential has no general analytic time-dependent solution. However, in one dimension the steady state can be determined analytically and is given by [2]

$$P_S(x) = \frac{1}{Z} e^{-V(x)/\Theta} \int_x^{x+a} dx' e^{V(x')/\Theta}, \tag{6}$$

where

$$Z = \int_0^a dx \int_x^{x+a} dx' \, e^{[V(x')-V(x)]/\Theta}. \tag{7}$$

The average velocity can also be determined exactly and is [2]

$$v_S = \frac{\Theta a}{\gamma Z}(1 - e^{-fa/\Theta}). \tag{8}$$

III. TIGHT-BINDING METHOD

The tight-binding method is a basis discretization method that allows the continuous diffusion equation [Eq. (1)] for overdamped Brownian motion on a tilted periodic potential to be systematically transformed to a simpler discrete master equation. The method applies for periodic and tilted periodic potentials that have only one dominant minimum per period that is deep compared to the thermal energy. The main benefits of the method are that it provides formal expressions for the rate of hopping between discrete states and it makes clear the validity of the master equation description. We present here a brief summary of the tight-binding method. Full details can be found elsewhere [13,14].

The evolution operator $\mathcal{L}$ for a tilted periodic potential is not, in general, Hermitian. A biorthonormal set can be constructed from the eigenfunctions of the evolution operator $\mathcal{L}$ and its adjoint $\mathcal{L}^\dagger = (1/\gamma)[\Theta\partial^2/\partial x^2 + F(x)\partial/\partial x]$. The eigenfunctions $\phi_{\alpha,k}(x)$ of $\mathcal{L}$ satisfy the eigenequations [1]

$$\mathcal{L}\phi_{\alpha,k}(x) = -\lambda_{\alpha,k}\phi_{\alpha,k}(x), \tag{9}$$

and the adjoint eigenfunctions $\phi^\dagger_{\alpha,k}(x)$ of $\mathcal{L}^\dagger$ satisfy

$$\mathcal{L}^\dagger\phi^\dagger_{\alpha,k}(x) = -\lambda^\dagger_{\alpha,k}\phi^\dagger_{\alpha,k}(x). \tag{10}$$

The eigenvalues $\lambda^\dagger_{\alpha,k} = \lambda^*_{\alpha,k}$ are imaginary, in general [1,14]. Due to the periodicity of $F(x)$, the eigenvalues separate into bands and the eigenfunctions have the Bloch form [13,14,17]

$$\phi_{\alpha,k}(x) = e^{ikx}u_{\alpha,k}(x), \tag{11}$$

$$\phi^\dagger_{\alpha,k}(x) = e^{ikx}u^\dagger_{\alpha,k}(x), \tag{12}$$

where the functions $u_{\alpha,k}(x+a) = u_{\alpha,k}(x)$ and $u^\dagger_{\alpha,k}(x+a) = u^\dagger_{\alpha,k}(x)$ are periodic with periodicity a, α is the band index, and k is the wave number restricted to the first Brillouin zone [17]. The ground state $\phi_{0,0}(x)$ is periodic with periodicity a and $\lambda_{0,0} = 0$ [1].

For potentials with deep minima compared to the thermal energy Θ, the system for long times becomes localized around minima of the potential. In that case, the delocalized eigenfunctions are not a convenient basis. Instead, the system can be expanded in the localized Wannier states

$$w_{\alpha,n}(x) = \frac{1}{q}\int_B dk \, \phi_{\alpha,k}(x)e^{-ikan}, \tag{13}$$

$$w^\dagger_{\alpha,n}(x) = \frac{1}{q}\int_B dk \, \phi^\dagger_{\alpha,k}(x)e^{-ikan}, \tag{14}$$

where $q = 2\pi/a$ and n is an integer [14]. The Wannier states are a real, discrete, and biorthonormal set [1,14]. Expanding the probability density as

$$P(x,t) = q\sum_{\alpha,n} p_{\alpha,n}(t)w_{\alpha,n}(x), \tag{15}$$

where $p_{\alpha,n}(t) = \int dx \, w^\dagger_{\alpha,n}(x)P(x,t)$, the Wannier states transform the continuous Smoluchowski equation [Eq. (1)] to a discrete evolution equation describing hopping between Wannier states within the same band [13,14].

To derive a discrete master equation, the following approximations are applied. Approximation (A1): The eigenstates in higher bands decay rapidly and are neglected for long times [13]. In this approximation, only the lowest band is retained and, dropping the α subscript, the full discrete evolution equation reduces to the master equation,

$$\frac{\partial p_n(t)}{\partial t} = \sum_{n'} \kappa_{n-n'} p_{n'}(t), \tag{16}$$

where the hopping rates are

$$\kappa_n = -\frac{1}{q}\int_B dk \, \lambda_k e^{ikan}, \tag{17}$$

and $\sum_n \kappa_n = -\lambda_0 = 0$ [14]. Approximation (A2): The Wannier states in the lowest band are well localized and hopping transitions beyond nearest-neighbor Wannier states are neglected. In this approximation, the sum in the master equation [Eq. (16)] is truncated, retaining only κ_n with $n = -1,0,1$. Approximation (A3): For deep minima, the nearest-neighbor hopping rates $\kappa_{\pm1}$ are approximated by Kramers' escape rate [14,15],

$$\kappa_{\rm K} = \frac{\sqrt{-V''(x_{\rm max})V''(x_{\rm min})}}{2\pi\gamma} e^{-[V(x_{\rm max})-V(x_{\rm min})]/\Theta}, \tag{18}$$

where $x_{\rm min}$ is the position of the minimum initially occupied, and $x_{\rm max}$ is the position of the potential maximum that must be escaped to reach the minimum finally occupied. The tilt dependence of the nearest-neighbor hopping rates can be further approximated by truncating Kramers' escape rate Eq. (18) to lowest order to yield [14,16]

$$\kappa^{\rm T}_{\pm1} \approx e^{\pm\alpha_{\pm1}fa/\Theta}\kappa^0_{\rm K}, \tag{19}$$

where $\kappa^0_{\rm K}$ is Kramers' escape rate for $f = 0$ and $\alpha_{\pm1}$ are the loading coefficients describing the relative position of potential

maxima between consecutive minima. The loading coefficients satisfy $0 \leqslant \alpha_{\pm 1} \leqslant 1$ and $\alpha_1 + \alpha_{-1} = 1$.

IV. NUMERICS

We implement the tight-binding method for specific potentials, as follows. The eigenfunctions $\phi_{\alpha,k}$ and eigenvalues $\lambda_{\alpha,k}$ are determined numerically by expanding the periodic functions $u_{\alpha,k}(x)$ of the Bloch states Eq. (11) according to [12]

$$u_{\alpha,k}(x) = \sum_n c_{n,\alpha,k} e^{inqx}. \tag{20}$$

We impose periodic boundary conditions with period Na where N is a large integer ($N \gtrsim 32$). Diagonalizing the matrix equation for the coefficients $c_{n,\alpha,k}$, we construct the eigenfunctions $\phi_{\alpha,k}(x)$ and determine the lowest band Wannier states $w_n(x)$ using Eq. (13). The phases of the Bloch eigenfunctions are chosen to vanish at the nth potential minimum so that the Wannier states in the lowest band are localized [18]. The adjoint eigenfunctions $\phi^\dagger_{\alpha,k}(x)$ and Wannier states $w^\dagger_n(x)$ can be determined similarly. We normalize according to the orthonormality relation [1,12,14]

$$\frac{q}{N}\int_0^{Na} dx\ \phi^{\dagger *}_{\alpha,k}(x)\phi_{\alpha',k'}(x) = \delta_{\alpha\alpha'}\delta_{kk'}. \tag{21}$$

For tilted periodic potentials, i.e., $f \neq 0$, Eq. (21) does not on its own determine the relative weighting of the eigenfunctions and their adjoints. Therefore, we also take

$$\frac{q}{N}\int_0^{Na} dx\ \frac{\phi^*_{\alpha,k}(x)\phi_{\alpha',k'}(x)}{\phi_{0,0}(x)} = \delta_{\alpha\alpha'}\delta_{kk'}. \tag{22}$$

When $f = 0$, the adjoint states have the form $\phi^\dagger_{\alpha,k}(x) = \phi_{\alpha,k}(x)/\phi_{0,0}(x)$ [1] and Eq. (22) reproduces Eq. (21).

We consider four periodic potentials that have periodicity a, amplitude A, and deep minima centered around zero. These are (i) the cosine potential,

$$V_0^{\cos}(x) = -\frac{A}{2}\cos(qx) + \frac{A}{2}; \tag{23}$$

(ii) the asymmetric ratchet potential,

$$V_0^{\rm rat}(x) = -\frac{B}{2}\cos[q(x-x_0)] + \frac{B}{8}\sin[2q(x-x_0)] + \frac{A}{2}, \tag{24}$$

where

$$B = \frac{4\sqrt{2}A}{\sqrt[4]{3}(3+\sqrt{3})} \tag{25}$$

and

$$qx_0 = -\arcsin\left(\frac{1-\sqrt{3}}{2}\right); \tag{26}$$

(iii) the maxima-broadened potential,

$$V_0^{\rm bro}(x) = -\frac{A}{2}\cos(qx) - \frac{A}{8}\cos(2qx) + \frac{5A}{8}; \tag{27}$$

and (iv) the double-minima potential,

$$V_0^{\rm dou}(x) = -\frac{C}{2}\cos(qx) + \frac{C}{8}\cos(4qx) + \frac{(1+\sqrt{5})A}{5+\sqrt{5}}, \tag{28}$$

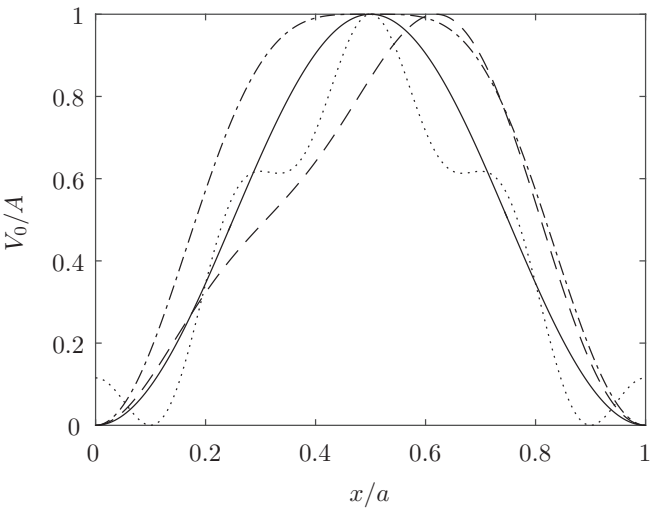

FIG. 1. (Solid) Cosine potential Eq. (23), (dashed) asymmetric ratchet potential Eq. (24), (dashdot) maxima-broadened potential Eq. (27), and (dotted) double-minima potential Eq. (28).

where

$$C = \frac{32A}{5(5+\sqrt{5})}. \tag{29}$$

The potentials are shown in Fig. 1. For large values of A, the potentials (ii) and (iv) can, particularly when tilted, have multiple deep minima per period. In this paper, we restrict our discussion to cases where the potentials have only one dominant deep minimum per period.

V. EQUILIBRIUM

For untilted periodic potentials with $f = 0$ the system is in thermal equilibrium. Figure 2 shows the lowest eigenvalue bands for the potentials shown in Fig. 1. The eigenvalues $\lambda_{\alpha,k}$

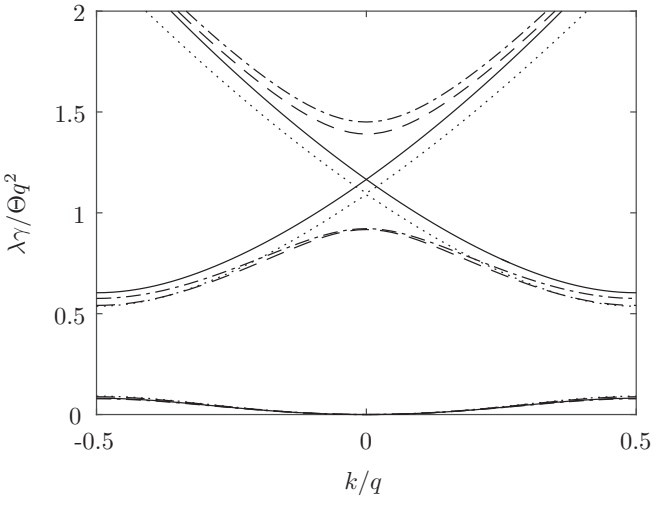

FIG. 2. Lowest eigenvalues for the untilted (solid) cosine potential Eq. (23), (dashed) asymmetric ratchet potential Eq. (24), (dashdot) maxima-broadened potential Eq. (27), and (dotted) double-minima potential Eq. (28) with $A = 2\Theta$.

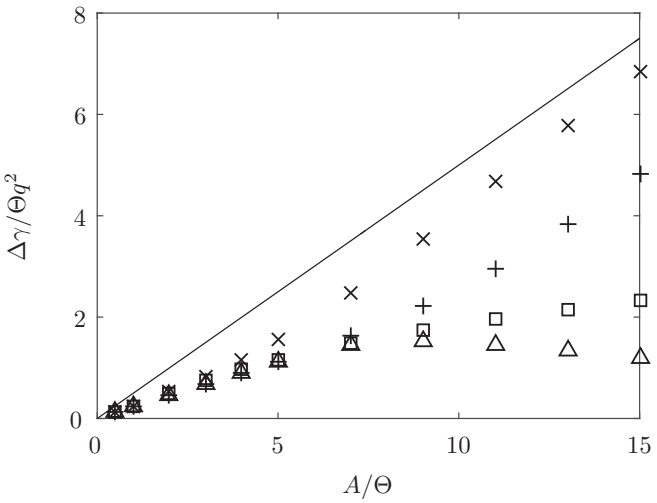

FIG. 3. Band gap Δ between the two lowest eigenvalue bands for the untilted ($\times$) cosine potential Eq. (23), ($+$) asymmetric ratchet potential Eq. (24), ($\square$) maxima-broadened potential Eq. (27), and ($\triangle$) double-minima potential Eq. (28). The solid curve is the analytic result Eq. (31) based on the harmonic approximation to the minima of the cosine potential.

are real and even in k [13]. In the limit of deep potential minima, i.e., $A \gg \Theta$, the lowest eigenvalue band has the tight-binding form

$$\lambda_k = 2\kappa_1[1 - \cos(ka)], \tag{30}$$

derived by inverting the hopping rates Eq. (17) and assuming nearest-neighbor hopping. The gap $\Delta = \lambda_{1,\pm q/2} - \lambda_{0,\pm q/2}$ between the lowest two eigenvalue bands is shown in Fig. 3 and typically increases with A/Θ. For the cosine potential, the gap is on the order of the separation between the two lowest eigenvalues of the harmonic approximation to the potential minima, i.e.,

$$\Delta \approx \frac{V_0''(0)}{\gamma} = \frac{Aq^2}{2\gamma}. \tag{31}$$

The hopping rates κ_n are determined from the eigenvalues by Eq. (17) and for $f = 0$ the symmetry of the eigenvalues means that $\kappa_n = \kappa_{-n}$ [13]. The nearest-neighbor hopping rates κ_1 are shown in Fig. 4(a) for the potentials in Fig. 1. These rates decrease for increasing A/Θ and determine the height of the lowest eigenvalue band [see Eq. (30)]. A comparison between κ_1 and Kramers' escape rate κ_K of Eq. (18) is given in Figs. 4(a) and 4(b) for the cosine and ratchet potentials. Kramers' escape rate is not directly applicable to potentials (iii) and (iv) because it requires a single maximum and minimum per period and a finite curvature at these extrema. For deep potentials we find good quantitative agreement between the nearest-neighbor hopping rates and Kramers' escape rate. Furthermore, Kramers' escape rate for a cosine potential provides reasonable qualitative agreement for all the potentials considered.

The hopping rates κ_n with $|n| > 1$ are the rates of higher-order transitions, i.e., $\kappa_{\pm 2}$ describes the rate of hopping

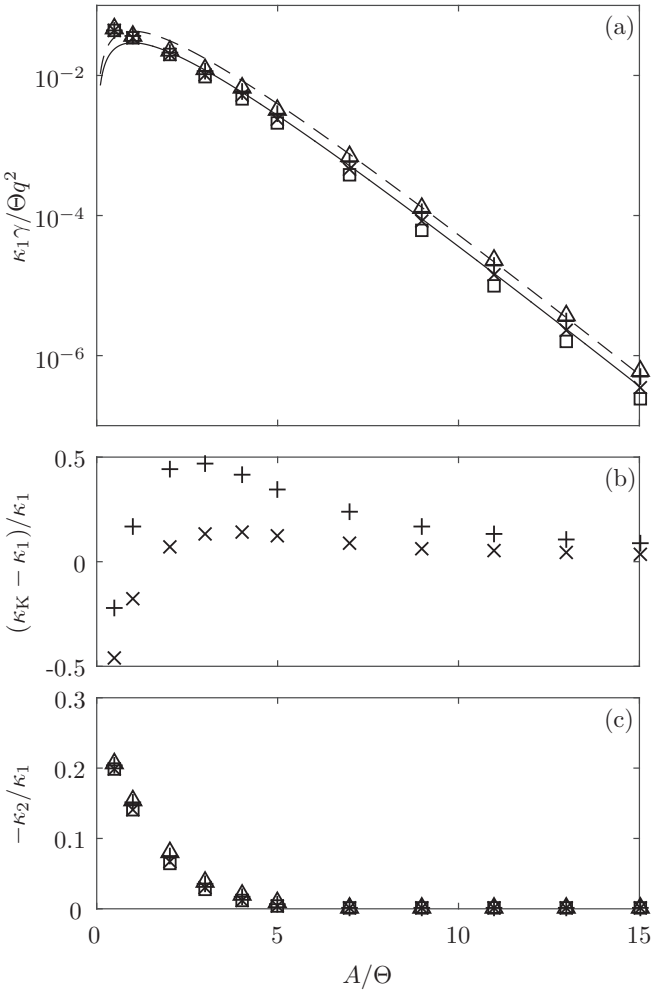

FIG. 4. (a) Nearest-neighbor hopping rate κ_1, (b) fractional difference between Kramers' escape rate Eq. (18) and κ_1, and (c) ratio $-\kappa_2/\kappa_1$ for the untilted ($\times$) cosine potential Eq. (23), ($+$) asymmetric ratchet potential Eq. (24), ($\square$) maxima-broadened potential Eq. (27), and ($\triangle$) double-minima potential Eq. (28). The curves in (a) are Kramers' escape rate for the untilted (solid) cosine potential and (dashed) asymmetric ratchet potential.

between next-nearest-neighbor states, $\kappa_{\pm 3}$ describes the rate of transitions between Wannier states separated by $3a$, etc. The higher-order hopping rates decrease in magnitude with increasing A/Θ and $|n|$. They are positive for odd $|n|$ and negative for even $|n|$. The higher-order hopping rates are negligible for deep potential minima but become important as A/Θ decreases. In the limit $A \to 0$, the hopping rates can be found by inserting the parabolic form $\lambda_k = \Theta k^2/\gamma$ of the eigenvalues into Eq. (17) to yield

$$\kappa_n\gamma/\Theta q^2 = -\frac{(-1)^{|n|}}{2\pi^2 n^2}, \quad \text{for } |n| > 0, \tag{32}$$

$$\kappa_0\gamma/\Theta q^2 = -\frac{1}{12}. \tag{33}$$

Figure 4(c) shows the second-order hopping rates κ_2 for the potentials shown in Fig. 1.

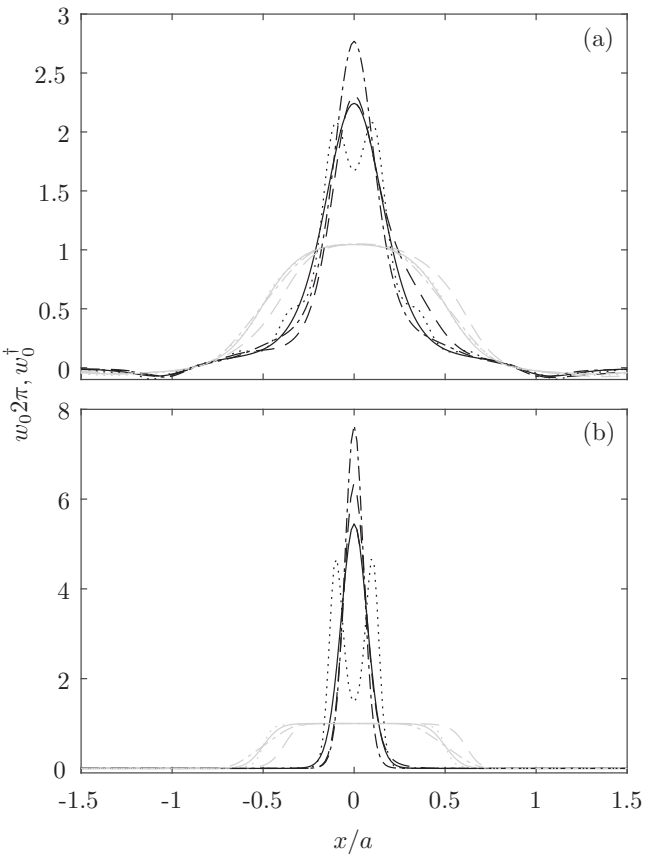

FIG. 5. (Black) Wannier state $w_0(x)$ and (gray) adjoint state $w_0^\dagger(x)$ for the untilted (solid) cosine potential Eq. (23), (dashed) asymmetric ratchet potential Eq. (24), (dash-dot) maxima-broadened potential Eq. (27), and (dotted) double-minima potential Eq. (28) with (a) $A = 2\Theta$ and (b) $A = 10\Theta$.

The lowest band Wannier states $w_0(x)$ and the adjoint states $w_0^\dagger(x) \propto \exp[V_0(x)/\Theta]w_0(x)$ are shown in Fig. 5. For deep potential minima, the Wannier states are well localized and for potentials with a single minimum per period are well approximated by the Gaussian ground state of the harmonic approximation to the potential minimum. For the double-minima potential Eq. (28) the Wannier state has two peaks. As A/Θ decreases the Wannier states become increasingly delocalized, gaining negative peaks at $x = \pm a$ and eventually tending to the sinc function $w_0(x) \propto \sin(qx/2)/x$ in the limit $A \to 0$. The adjoint Wannier states are broader localized functions that are approximately one in the region where the Wannier states are localized. Like the Wannier states, the adjoint states become increasingly delocalized for decreasing A/Θ tending to sinc functions in the limit $A \to 0$. The standard deviation

$$\sigma = \sqrt{\int dx\, x^2 |f(x)| - \left[\int dx\, x |f(x)|\right]^2}, \qquad (34)$$

where the function $f(x)$ is replaced by the Wannier states or their adjoints is shown in Fig. 6. The delocalization of the Wannier states with decreasing A/Θ is reflected in the increase in magnitude of the second-order hopping rates $\kappa_{\pm 2}$ [see Fig. 4(c)].

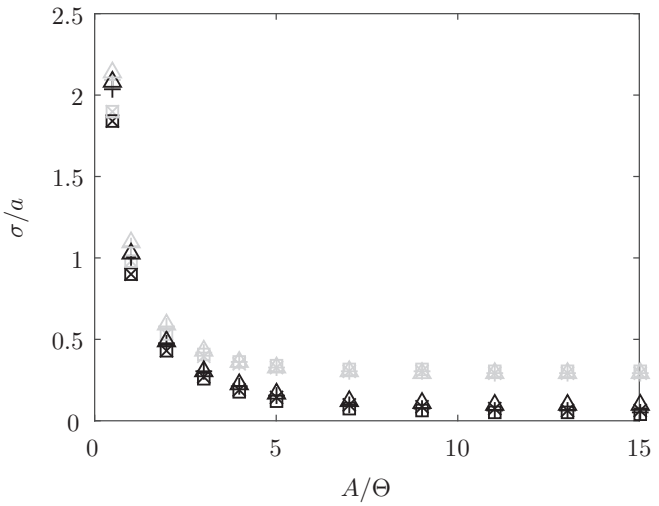

FIG. 6. Standard deviation σ of the absolute value of the (black) Wannier state $w_0(x)$ and (gray) adjoint state $w_0^\dagger(x)$ for the untilted (×) cosine potential Eq. (23), (+) asymmetric ratchet potential Eq. (24), (□) maxima-broadened potential Eq. (27), and (△) double-minima potential Eq. (28).

VI. NONEQUILIBRIUM

For tilted periodic potentials with $f \neq 0$ the system is driven out of thermal equilibrium. Figure 7 shows the band structure for the potentials shown in Fig. 1. The eigenvalues $\lambda_{\alpha,k}$ are imaginary with an even real part [see Fig. 7(a)] and an odd imaginary part [see Fig. 7(b)]. The imaginary part

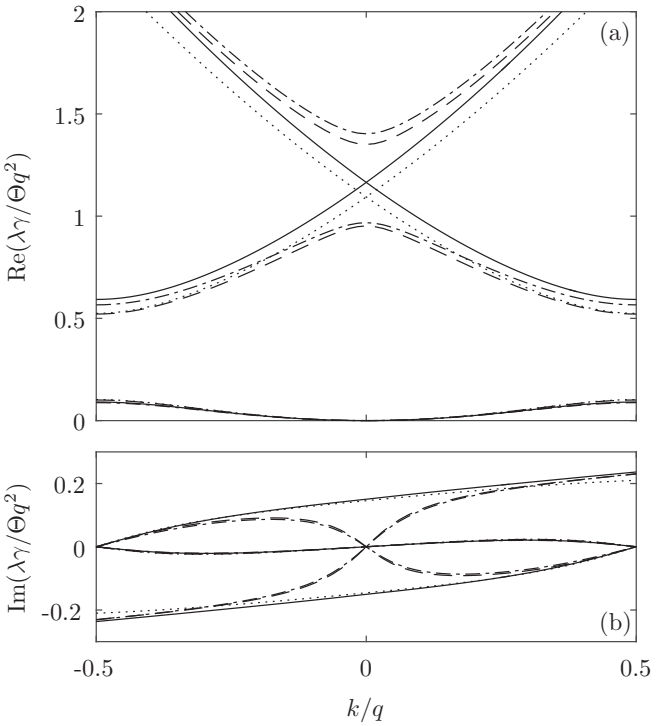

FIG. 7. (a) Real and (b) imaginary parts of the lowest eigenvalues for the tilted (solid) cosine potential Eq. (23), (dashed) asymmetric ratchet potential Eq. (24), (dashdot) maxima-broadened potential Eq. (27), and (dotted) double-minima potential Eq. (28) with $A = 2\Theta$ and $f = \Theta/a$.

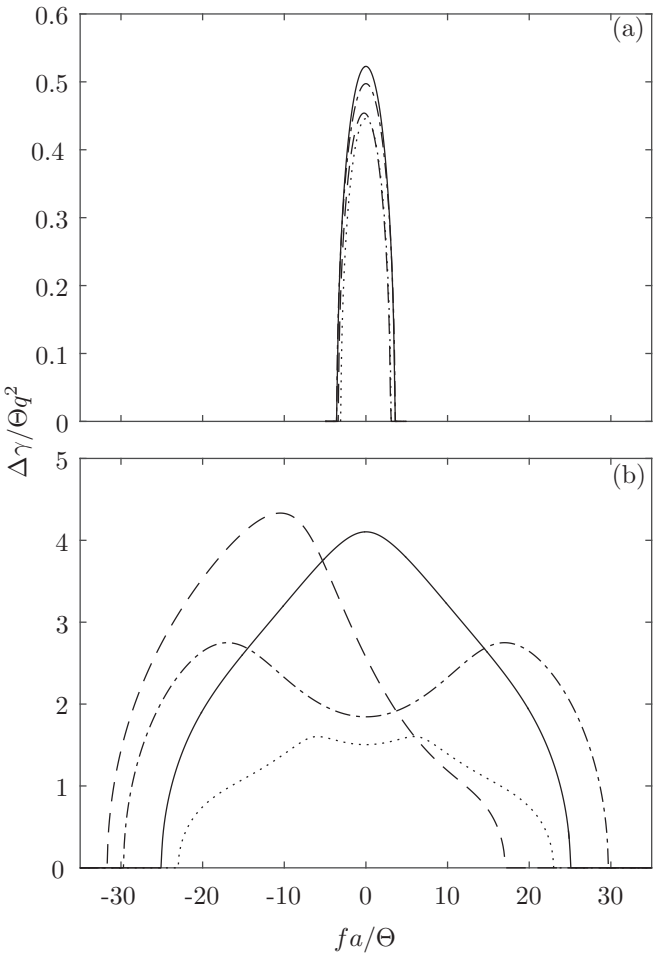

FIG. 8. Band gap Δ between the two lowest eigenvalue bands for the tilted (solid) cosine potential Eq. (23), (dashed) asymmetric ratchet potential Eq. (24), (dashdot) maxima-broadened potential Eq. (27), and (dotted) double-minima potential Eq. (28) with (a) $A = 2\Theta$ and (b) $A = 10\Theta$.

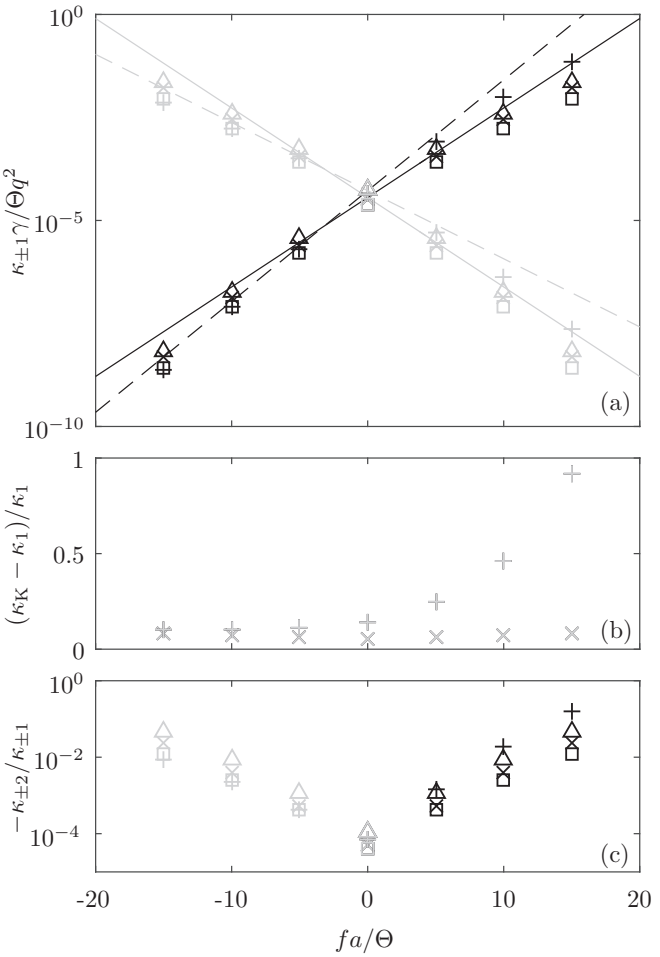

FIG. 9. (a) Nearest-neighbor hopping rates (black) κ_1 and (gray) κ_{-1}, (b) fractional difference between Kramers' escape rate Eq. (18) and κ_1, and (c) ratio (black) $-\kappa_2/\kappa_1$ and (gray) $-\kappa_{-2}/\kappa_{-1}$ for the tilted ($\times$) cosine potential Eq. (23), ($+$) asymmetric ratchet potential Eq. (24), ($\square$) maxima-broadened potential Eq. (27), and ($\triangle$) double-minima potential Eq. (28) with $A = 10\Theta$. The curves in (a) are the truncated Kramers' escape rate Eq. (19) for the tilted (solid) cosine potential and (dashed) asymmetric ratchet potential.

vanishes when there is a gap in the real part. In the limit of deep potential minima, i.e., $A \gg \Theta$ and $A \gg fa$, the lowest eigenvalue band has the form

$$\lambda_k = (\kappa_1 + \kappa_{-1})(1 - \cos ka) + i(\kappa_1 - \kappa_{-1}) \sin ka. \quad (35)$$

Figure 8 shows the gap $\Delta = \lambda_{1,\pm q/2} - \lambda_{0,\pm q/2}$ between the lowest two bands. The gap typically decreases with increasing tilt until it vanishes. For $A \gg \Theta$ the gap vanishes when the barrier height falls below Θ. As A/Θ decreases the gap is maintained for barrier heights less than Θ. The tilt dependence of the gap is asymmetric for the asymmetric ratchet potential Eq. (24).

The hopping rates κ_n are tilt dependent and are shown in Fig. 9. For $n > 0$ ($n < 0$) the nearest-neighbor rates increase (decrease) in magnitude for increasing fa/Θ. The truncated Kramers' escape rate Eq. (19) captures general features of the tilt dependence of the nearest-neighbor hopping rates and provides quantitative agreement for $fa \ll A$ [see Fig. 9(a)]. The full Kramers' escape rate Eq. (18) provides reasonable quantitative agreement across a wide range of tilting for the cosine potential [see Fig. 9(b)]. The agreement is not as good for the asymmetric ratchet potential because the potential minima become shallow very quickly for increasing positive f. The second-order hopping rates $\kappa_{\pm2}$ are shown in Fig. 9(c). They are negligible for deep potential minima but increase in magnitude exponentially with increasing $|f|$.

The lowest band Wannier states and their adjoints are shown in Fig. 10. As in the $f = 0$ case, the Wannier states are centered on potential minima and for deep minima are well localized. The standard deviations are shown in Fig. 11. These increase slowly with increasing $|f|$ until the potential minima become shallow compared to Θ and the Wannier states become delocalized.

VII. VALIDITY

The tight-binding derivation of the discrete master equation [Eq. (16)] uses three approximations: (A1) the truncation to the lowest band, (A2) the truncation to nearest-neighbor hopping, and (A3) the use of Kramers' escape rate for the nearest-

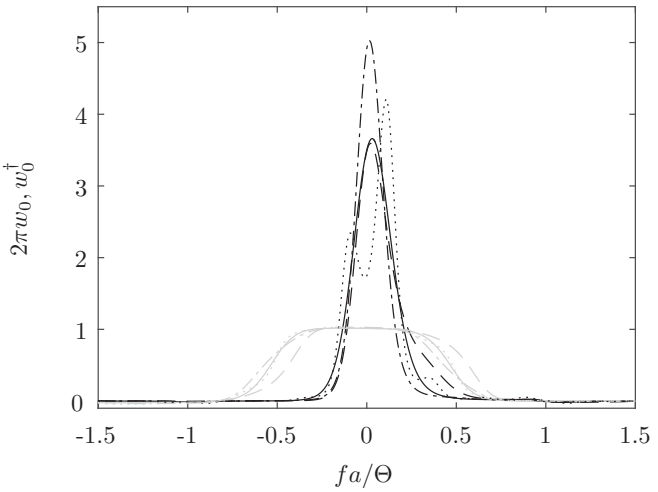

FIG. 10. (Black) Wannier state $w_0(x)$ and (gray) adjoint state $w_0^\dagger(x)$ for the tilted (solid) cosine potential Eq. (23), (dashed) asymmetric ratchet potential Eq. (24), (dash-dot) maxima-broadened potential Eq. (27), and (dotted) double-minima potential Eq. (28) with $A = 5\Theta$ and $f = 3\Theta/a$.

neighbor hopping rates. In general, these approximations are valid for long times and deep potential minima. However, having calculated in Secs. V and VI the band gap, hopping rates, and Wannier states for a variety of potentials, further details of the validity of the tight-binding method can be provided, as follows.

In Approximation (A1), the states above the lowest band are truncated. This requires a separation of timescales, i.e., the band gap in the eigenvalue spectrum needs to be large compared to the height of the real part of the lowest band. For $f = 0$ and $A > 1$, the gap is larger than the height of the lowest band and for increasing A the gap increases while the height of the lowest band decreases. With increasing $|f|$ the gap is relatively slowly varying until it drops to zero rapidly in the region where the potential becomes monotonically increasing or decreasing. Therefore, provided a gap exists, it is reasonable to assume a lowest-band description in the long-time limit.

In Approximation (A2), hopping beyond nearest neighbors is neglected. This requires the Wannier states in the lowest band to be sufficiently localized that the second-order hopping rates $\kappa_{\pm 2}$ are negligible. If the (negative) second-order hopping rates are not negligible then they appear in the master equation. In that case the master equation no longer takes the standard form with positive rates. Therefore, for a valid master equation, and an interpretation of the system dynamics in terms of hopping between localized states, the second-order rates must be negligible compared to the first-order rates.

In Approximation (A3), the nearest-neighbor hopping rates are determined by Kramers' escape rate. Kramers' escape rate Eq. (18) and the truncated rate Eq. (19) provide a reasonable qualitative description of the hopping rates in the regime where the discrete master equation is valid [i.e., when Approximations (A1) and (A2) hold]. However, good quantitative agreement with Kramers' escape rate is only possible for certain potentials and requires deeper potential minima than is necessary for a valid discrete master equation treatment, as detailed further below.

Figure 12 shows the hierarchy of approximations for the cosine potential Eq. (23). The color map relates to Approximation (A3) and shows the difference between Kramers' escape rate Eq. (18) and the nearest-neighbor rate κ_1. The map is approximately symmetric in f and has a lower bound at the critical tilt [19], where the potential becomes monotonically increasing or decreasing with no maxima or minima. The dashed curve shows the lower bound of the region where the truncated Kramers' escape rate Eq. (19) agrees with the nearest-neighbor hopping rates to within 10%. The solid curve relates to Approximation (A2) and shows where the second-order hopping rates are 1% of the first-order rates.

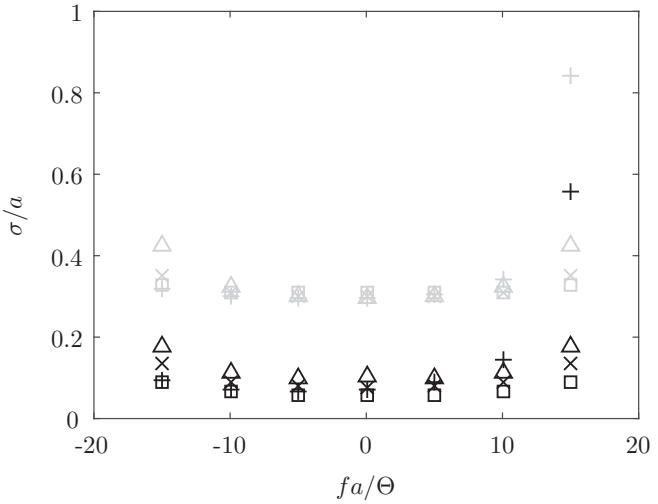

FIG. 11. Standard deviation σ of the absolute value of the (black) Wannier state $w_0(x)$ and (gray) adjoint state $w_0^\dagger(x)$ for the tilted (×) cosine potential Eq. (23), (+) asymmetric ratchet potential Eq. (24), (□) maxima-broadened potential Eq. (27), and (△) double-minima potential Eq. (28) with $A = 10\Theta$.

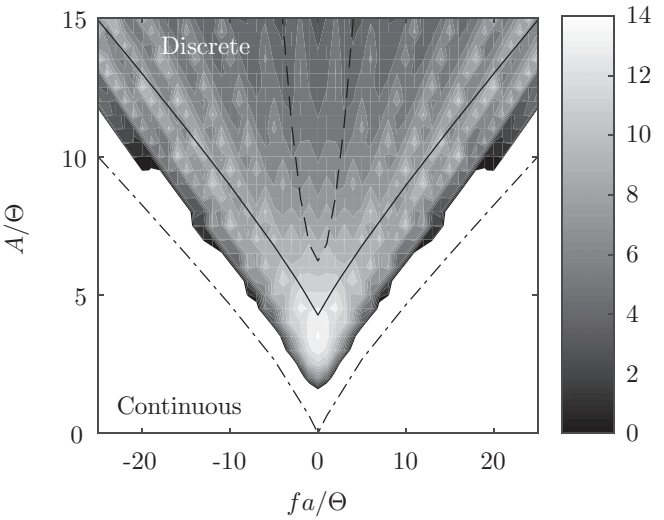

FIG. 12. Fractional difference $100(\kappa_K - \kappa_1)/\kappa_1$ for the tilted cosine potential Eq. (23). The curves are where (solid) $-\kappa_{\mathrm{sgn}(f)2}/\kappa_{\mathrm{sgn}(f)1}$ is 0.01, (dashed) $(\kappa_1^T - \kappa_1)/\kappa_1$ is 0.1, and (dash-dot) the gap Δ vanishes.

Above the solid curve the discrete master equation with nearest-neighbor hopping can be considered valid while below the solid curve the continuous diffusion equation is more appropriate. In the region between the solid and dashed curves, the master equation is valid but the nearest-neighbor hopping rates are not well described by the truncated Kramers' escape rate Eq. (19). In that regime, either the full Kramers' rate Eq. (18) can be used or, more accurately, the hopping rates can be determined from the lowest-band eigenvalues according to Eq. (17). The dash-dot curve relates to Approximation (A1) and shows the lower bound of the region where the eigenvalue spectrum is gapped. This lies below the solid-curve boundary of Approximation (A2).

In summary, Approximations (A1) and (A2) are required for a discrete master equation treatment to be valid. Approximation (A2) is a tighter constraint than Approximation (A1). Therefore, provided the next-nearest neighbor hopping rates are negligible, a master equation can be used. The nearest-neighbor hopping rates are well described qualitatively by Kramers' escape rate. The full Kramers' escape rate Eq. (18) is quantitative over a wider regime than the truncated rate Eq. (19), but both expressions require deeper potential minima than Approximations (A1) and (A2). In the regime where a discrete maser equation treatment is valid but Kramers' escape rate is not quantitative, i.e., Approximations (A1) and (A2) hold but (A3) does not, Kramers' escape rate overestimates the rate of hopping between neighboring Wannier states.

VIII. COMPARISON WITH THE EXACT STEADY STATE

In the regime where the discrete master equation is valid, the tight-binding method can be used to determine steady-state properties of the system. Here we use the tight-binding method to determine the ground state and average drift and we compare our results with exact analytic results for the steady state [see Sec. II].

The master equation Eq. (16) can be solved analytically by transforming to the diagonal form using $c_k(t) = \sum_n p_n(t)\exp(-ikan)$ [13]. In the ground state, $p_n(t)$ is independent of n and t and, using the expansion Eq. (15), the ground state has the form

$$\phi_0(x) \propto \sum_n w_n(x). \tag{36}$$

Given the localization of the Wannier states $w_n(x)$, the ground state in a single period a is well approximated by truncating the sum in Eq. (36) to the appropriate single value of n where the Wannier state $w_n(x)$ is localized on that period. Therefore, the Wannier state $w_0(x)$ provides a good description of the ground state in the region $-a/2 \leqslant x \leqslant a/2$ [see Figs. 5 and 10]. To compare the ground state Eq. (36) with the exact steady-state probability density Eq. (6), we calculate [12]

$$\Delta P = \int_{-a/2}^{a/2} dx\, |P_S(x) - \phi_0(x)|, \tag{37}$$

where both the steady state $P_S(x)$ and the ground state $\phi_0(x)$ are normalized to unity over the region of integration in Eq. (37). Figure 13 shows ΔP for a range of tilting. We find that truncating the sum in Eq. (36) to a single Wannier state $n = 0$ provides good agreement with the steady-state solution

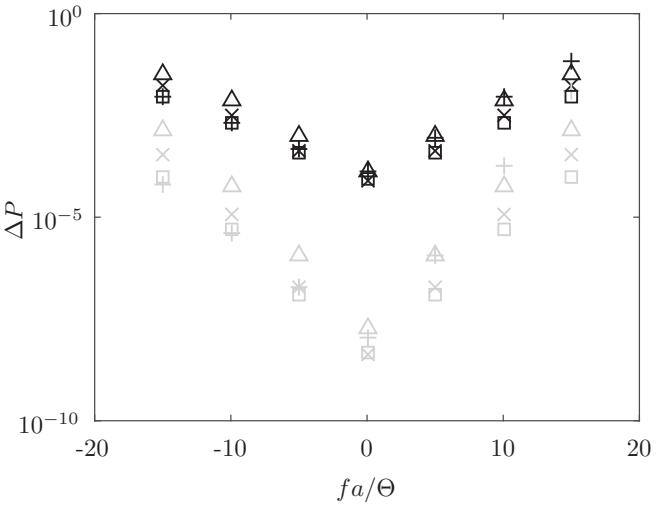

FIG. 13. Comparison ΔP of Eq. (37) between the exact steady state Eq. (6) and the ground state Eq. (36) taking the sum over (black) $n = 0$ and (gray) $n = 0, \pm 1$ for the tilted ($\times$) cosine potential Eq. (23), ($+$) asymmetric ratchet potential Eq. (24), ($\square$) maxima-broadened potential Eq. (27), and ($\triangle$) double-minima potential Eq. (28) with $A = 10\Theta$.

within the regime of validity of the master equation treatment [Approximations (A1) and (A2)]. The deviation from the exact steady-state solution increases with the magnitude of the tilt, reflecting the delocalization of the Wannier states [see Fig. 11] and breakdown of the master equation approach as the second-order hopping rates increase in magnitude [see Fig. 9(c)]. Calculating the ground state $\phi_0(x)$ using $n = 0, \pm 1$ in the sum in Eq. (36) provides better agreement with the steady state, as shown in gray in Fig. 13.

The average drift v can be calculated from the nearest-neighbor hopping rates in the master equation Eq. (16) according to [13]

$$v = \sum_n an\kappa_n = a(\kappa_1 - \kappa_{-1}). \tag{38}$$

When Kramers' escape rate is valid, the *Kramers' drift* v_K can be calculated by replacing the hopping rates $\kappa_{\pm 1}$ in Eq. (38) by the Kramers' escape rate Eq. (18). Further approximating the Kramers' escape rate using the truncated rate Eq. (19) yields the truncated drift

$$v_T = na\kappa_K^0(e^{\alpha_1 fa/\Theta} - e^{-\alpha_{-1} fa/\Theta}). \tag{39}$$

Figure 14 compares the average drift v calculated using the tight-binding method, and the Kramers' drift v_K calculated using Kramers' escape rate, with the exact result v_S of Eq. (8). We find that the drift v from the tight-binding method is in good agreement with the exact steady-state velocity v_S [see Figs. 14(a) and 14(c)], within the regime of validity of the master equation treatment. In the regime where the master equation is valid but Kramers' escape rate does not provide quantitative agreement, the Kramers' drift overestimates the magnitude of the steady-state velocity [see Figs. 14(a) and 14(b)].

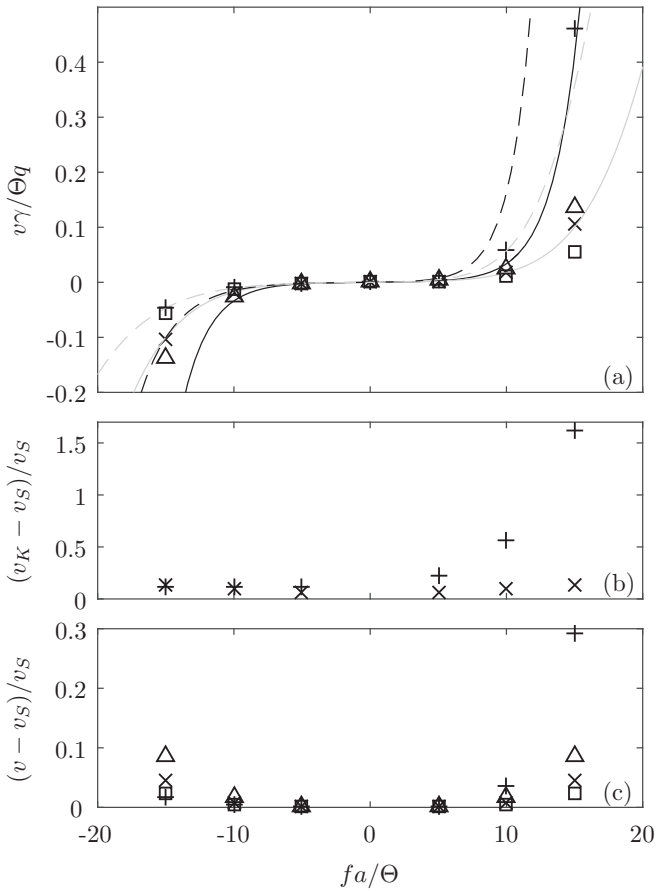

FIG. 14. (a) Steady-state drift v Eq. (38), (b) fractional difference between the Kramers' drift v_K and the exact steady-state drift v_S Eq. (8), and (c) fractional difference between the drift v and the exact steady-state drift v_S for the tilted (×) cosine potential Eq. (23), (+) asymmetric ratchet potential Eq. (24), (□) maxima-broadened potential Eq. (27), and (△) double-minima potential Eq. (28) with $A = 10\Theta$. The curves in (a) are (black) the drift v_T Eq. (39) calculated using the truncated Kramers' escape rate Eq. (19) and (gray) the exact steady-state drift v_S for the tilted (solid) cosine potential and (dashed) asymmetric ratchet potential.

IX. TWO DIMENSIONS

The tight-binding method can be applied to Brownian motion on periodic potentials in more than one dimension [13,14]. In addition to the validity considerations described above for one-dimensional systems, multidimensional systems are further complicated when the transition paths are not well defined. To illustrate the multidimensional case, we consider the simple two-dimensional nonseparable potential

$$V_0(x,y) = -\frac{A}{2}\cos(q_x x) - \frac{B}{2}\cos(q_y y) - \frac{C}{2}\cos(q_x x - q_y y) + \frac{A+B+C}{2}, \quad (40)$$

shown in Fig. 15. The potential has three spatially dependent terms. The term with amplitude A gives rise to processes occurring in the x direction alone, the term with amplitude B gives rise to processes occurring in the y direction alone, and the term with amplitude C couples the two dimensions [14,20].

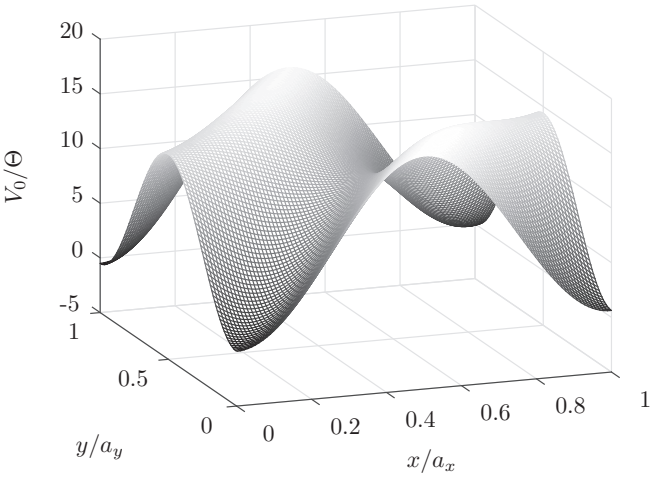

FIG. 15. Two-dimensional cosine potential Eq. (40) with $A/\Theta = 6$, $B/\Theta = 4$, and $C/\Theta = 10$.

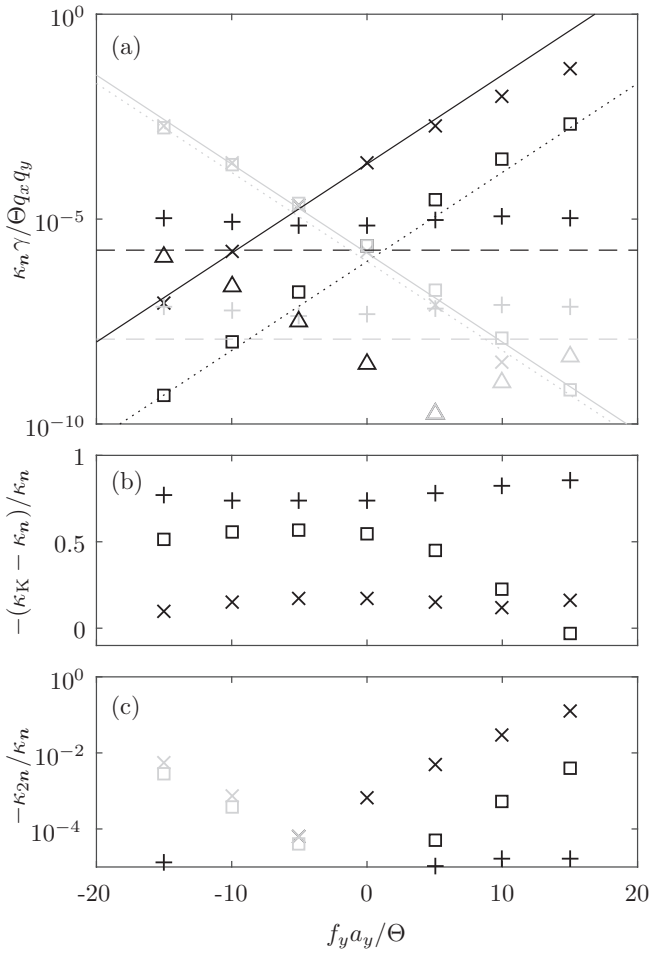

FIG. 16. (a) Nearest-neighbor hopping rates (black) $\kappa_{\boldsymbol{n}}$ and (gray) $\kappa_{-\boldsymbol{n}}$, (b) fractional difference between Kramers' escape rate Eq. (18) and $\kappa_{\boldsymbol{n}}$, and (c) ratio (black) $-\kappa_{2\boldsymbol{n}}/\kappa_{\boldsymbol{n}}$ and (gray) $\kappa_{-2\boldsymbol{n}}/\kappa_{-\boldsymbol{n}}$ for the two-dimensional tilted cosine potential Eq. (40) with $A/\Theta = 6$, $B/\Theta = 4$, $C/\Theta = 10$, and $f_x a_x/\Theta = 5$. The symbols are (×) $\boldsymbol{n} = (1,1)$, (+) (1,0), (□) (0,1), and (△)(1, − 1). The curves in (a) are the truncated Kramers' escape rate Eq. (19) for (solid) $\boldsymbol{n} = (1,1)$, (dashed) (1,0), and (dotted) (0,1).

We construct the potential with $C > A,B$ so the rates in the coupled direction dominate. We choose the friction coefficients such that $\gamma_x a_x^2 = \gamma_y a_y^2$ and we denote $\gamma = \sqrt{\gamma_x \gamma_y}$.

For deep potential minima, the two lowest eigenvalue bands are well separated and the lowest eigenvalue band has the tight-binding form

$$\lambda_{\boldsymbol{k}} = \sum_{\boldsymbol{n}} \kappa_{\boldsymbol{n}}[1 - \cos(\boldsymbol{k} \cdot \mathcal{A}\boldsymbol{n})] + i\kappa_{\boldsymbol{n}} \sin(\boldsymbol{k} \cdot \mathcal{A}\boldsymbol{n}), \qquad (41)$$

where $\boldsymbol{k} = (k_x,k_y)$, $\boldsymbol{n} = (n_x,n_y)$, and $\mathcal{A}$ is a diagonal matrix with $\mathcal{A}_{jj} = a_j$. The sum over $\boldsymbol{n}$ includes only the nearest-neighbor terms $\boldsymbol{n} = (\pm 1,0)$, $(0,\pm 1)$, and $(\pm 1,\pm 1)$. The terms with $\boldsymbol{n} = (\pm 1,\mp 1)$ are neglected as there is no part of the potential nonseparable in $q_x x + q_y y$. We find that for $A/\Theta = 6$, $B/\Theta = 4$, and $C/\Theta = 10$ the gap is more than four orders of magnitude larger than the height of the lowest band. The tilt dependence of the gap is qualitatively similar to the one-dimensional case (see the solid curves in Fig. 8), vanishing when the potential minima are no longer confined in all directions compared to the thermal energy Θ.

The hopping rates $\kappa_{\boldsymbol{n}}$ are shown in Fig. 16. The transition path in the coupled direction is tightly confined compared to the thermal energy Θ and also the barrier for hopping is large compared to Θ so Kramers' escape rate calculated using the minima and maxima of the transition path provides a reasonable description. In the x and y directions, Kramers' escape rate provides a reasonable qualitative description but the transition paths are weakly confined compared to Θ so Kramers' rate underestimates the hopping rates in these directions. The rates with $\boldsymbol{n} = (\pm 1,\mp 1)$ are negligible for $\boldsymbol{f} = \boldsymbol{0}$ but increase with increasing $|\boldsymbol{f}|$ [see Fig. 16(a)]. The next-nearest-neighbor hopping rates [see Fig. 16(c)] are negligible for deep potential minima and, as in the one-dimensional case, increase in magnitude with increasing $|\boldsymbol{f}|$.

X. CONCLUSION

We have presented a systematic numerical study of the tight-binding approach to overdamped Brownian motion on a tilted periodic potential. We have calculated the band structure, hopping rates, and Wannier states for a variety of potentials. For deep potential minima the Wannier states are well localized and the hopping rates between nearest-neighbor states are qualitatively well described by Kramers' escape rate. When Kramers' escape rate does not provide quantitative agreement, the tight-binding method enables the hopping rates between potential minima to be determined from the lowest-band eigenvalues of the system. The discrete master equation derived via the tight-binding method can be considered valid when the hopping rates between next-nearest-neighbor states are negligible compared to the nearest-neighbor hopping rates. The tight-binding method is also applicable in multiple dimensions.

It would be interesting to consider the implications of this work for specific physical systems described by Fokker-Planck equations [1,2,13,19]. For example, in one dimension the use of Kramers' escape rate can overestimate the nearest-neighbor hopping rates and the magnitude of the average drift. In the context of a strongly coupled molecular motor described by a discrete master equation [14,21], this would overestimate the power output and underestimate the efficiency at maximum power, although the efficiency at maximum power would remain bound by one half.

ACKNOWLEDGMENTS

This work has been supported by the Marsden Fund Council from Government funding, managed by the Royal Society of New Zealand (Contract No. FRI1401). The author thanks Michael W. Jack for helpful discussions and Robin Collignon for preliminary calculations.

[1] H. Risken, *The Fokker-Planck Equation. Methods of Solution and Applications*, 2nd ed. (Springer, Berlin, 1989).
[2] P. Reimann, Phys. Rep. **361**, 57 (2002).
[3] N. G. van Kampen, *Stochastic Processes in Physics and Chemistry* (Elsevier, North-Holland, 1981).
[4] C. W. Gardiner, *Stochastic Methods. A Handbook for the Natural and Social Sciences*, 4th ed. (Springer, Berlin, 2009).
[5] D. Chowdhury, Phys. Rep. **529**, 1 (2013).
[6] R. Ferrando, R. Spadacini, and G. E. Tommei, Phys. Rev. E **48**, 2437 (1993).
[7] P. Jung and B. J. Berne, in *New Trends in Kramers' Reaction Rate Theory*, edited by P. Talkner and P. Hänggi (Kluwer Academic, Netherlands, 1995), p. 67.
[8] G. Lattanzi and A. Maritan, Phys. Rev. E **64**, 061905 (2001).
[9] B. Lindner, M. Kostur, and L. Schimansky-Geier, Fluct. Noise Lett. **1**, R25 (2001).
[10] H. Wang, C. S. Peskin, and T. C. Elston, J. Theor. Biol **221**, 491 (2003).
[11] N. Golubeva, A. Imparato, and L. Peliti, Europhys. Lett. **97**, 60005 (2012).
[12] P. T. T. Nguyen, K. J. Challis, and M. W. Jack, Phys. Rev. E **93**, 022124 (2016).
[13] K. J. Challis and M. W. Jack, Phys. Rev. E **87**, 052102 (2013).
[14] K. J. Challis and M. W. Jack, Phys. Rev. E **88**, 042114 (2013).
[15] B. Caroli, C. Caroli, and B. Roulet, J. Stat. Phys. **21**, 415 (1979).
[16] A. B. Kolomeisky and M. E. Fisher, Annu. Rev. Phys. Chem. **58**, 675 (2007).
[17] C. Kittel, *Introduction to Solid State Physics* (Wiley, New York, 2004).
[18] W. Kohn, Phys. Rev. **115**, 809 (1959).
[19] P. Reimann, C. Van den Broeck, H. Linke, P. Hänggi, J. M. Rubi, and A. Pérez-Madrid, Phys. Rev. E **65**, 031104 (2002).
[20] M. O. Magnasco, Phys. Rev. Lett. **72**, 2656 (1994).
[21] C. Van den Broeck, N. Kumar, and K. Lindenberg, Phys. Rev. Lett. **108**, 210602 (2012).